First Hyperpolarizability of Water in Bulk Liquid Phase: Long-Range Electrostatic Effects Included via the Second Hyperpolarizability

Guillaume Le Breton, Oriane Bonhomme, Emmanuel Benichou, and Claire Loison*

University of Lyon, Université Claude Bernard Lyon 1, CNRS, Institut Lumière Matière, F-69622, Villeurbanne, France

E-mail: claire.loison@univ-lyon1.fr

Contents

S1   Methodological details

S1.1   Second hyperpolarizability calculation

Numerical Implementation:

To compute the second hyperpolarizability, we use the Finite Field (FF) method. The second hyperpolarizability is defined as the linear coefficient of the first hyperpolarizability evolution relative to an applied electrostatic field. For a vacuum calculation :

$$\gamma_{abcd}^{\text{vac}}(2\omega,\omega,\omega,0) = \frac{\delta\beta_{abc}^{\text{vac}}(2\omega,\omega,\omega)[e_d]}{\delta e_d}, \tag{S1}$$

where the dependence relative to the exciting frequency is noted with parentheses (), and the dependence relative to an external static field is noted with hooks []. For the PE calculations, the embedding creates an electric field $\mathbf{e}^{PE}$, and we define again γ in the PE embedding as the same derivative, but the field derivative is done around the field $\mathbf{e}^{PE}$.

$$\gamma_{abcd}^{PE}(2\omega,\omega,\omega,0) = \frac{\delta\beta_{abc}^{PE}(2\omega,\omega,\omega)[e_d]}{\delta e_d} \tag{S2}$$

The Equations S1 and S2 are written in the molecular frame: the first and second hyperpolarizability tensors β and γ are expressed in the molecular frame as well as the electrostatic field $\mathbf{e}$. Note that this electrostatic field $\mathbf{e}$ is **spatially-homogeneous** within the QM box, and is added to the one created by the PE environment. As a reminder, the later electrostatic field created by the environment $\mathbf{e}^{PE}$ can be **spatially-heterogeneous**. In the following, we omit the *PE* notation and the explicit adding of $\mathbf{e}^{PE}$ in the molecular frame, or $\mathbf{E}^{PE}$ in the laboratory frame. Practically, the components second hyperpolarizability components are obtained using linear fit:

$$\beta_{abc}(2\omega,\omega,\omega)[e_d^0] = \beta_{abc}(2\omega,\omega,\omega)[e_d^0 = 0] + \gamma_{abcd}(2\omega,\omega,\omega,0)e_d^0 \tag{S3}$$

$$\mathscr{B}ijk(2\omega,\omega,\omega)[E_l^0] = \mathscr{B}_{ijk}(2\omega,\omega,\omega)[E_l^0 = 0] + \Gamma_{ijkl}(2\omega,\omega,\omega,0)E_l^0, \tag{S4}$$

where $\mathscr{B}$ and Γ are the first and second hyperpolarizability in the laboratory frame, $\mathbf{E}$ is also expressed in the laboratory frame. All the quantities (first and second hyperpolarizabilities, electrostatic fields, etc.) are in atomic units.

For every molecule, several QM simulations are performed:

- One without extra electrostatic field, to get $\beta(2\omega, \omega, \omega)[0]$

- For every direction l, 6 QM calculations are performed with increasing electrostatic field, from 0.1 to 1.5×10^{-3} a.u. .

For each of these calculations, the hyperpolarizability tensor is computed: each simulation returns 27 components. To obtain the second hyperpolarizability component $ijkl$, the evolution of the hyperpolarizability component ijk is plotted with respect to the electric field along the l direction. For instance, in the Figure S1 is plotted the evolution of the β_{ccc} component in function of the electric field along the c direction. The slope of this linear evolution is the γ_{cccc} components. Globally, to obtain all the second hyperpolarizability components, we require 19 QM calculations per molecule.

We have verified that the linear dependency remains valid if the electrostatic finite field is directed in an arbitrary direction – data not shown. Within our range of electrostatic field applied (10^{-3} a.u. or 10^{-2} V.Å $^{-1}$):

$$\beta(2\omega, \omega, \omega)_{ijk}[\mathbf{e}] = \beta(2\omega, \omega, \omega)_{ijk}[0] + \sum_l \gamma_{ijkl}(2\omega, \omega, \omega, 0)\, e_l \qquad \text{(S5)}$$

Finally, to convert the second hyperpolarizability from the molecular to the laboratory frame, we use the rotational matrix R defined from the expression of the laboratory-frame unit vectors
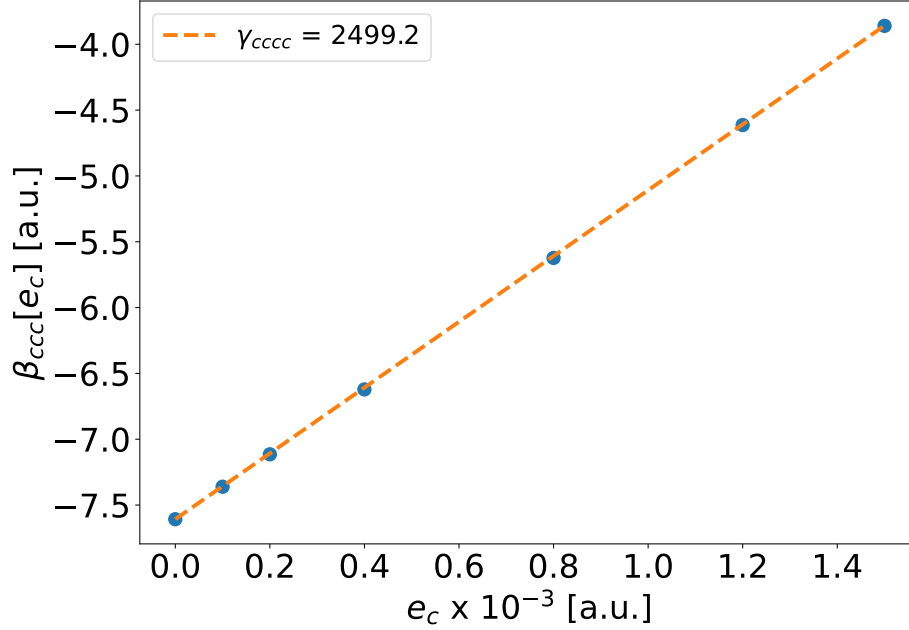
Figure S1: Evolution of one hyperpolarizability component as a function of the applied static and homogeneous electric field. Both hyperpolarizability and the electric field are expressed within the molecular frame. The obtained second hyperpolarizability component is shown in the legend, in atomic units.

$\mathbf{V}^{\text{lab}}$ in the molecular frame unit vectors $\mathbf{V}_a^{\text{mol}}$:

$$\mathbf{V}_i^{\text{lab}} = \sum_a R_{ia} \mathbf{V}_a^{\text{mol}}, \tag{S6}$$

$$\beta_{abc}(2\omega, \omega, \omega) = \sum_{ijk} R_{ai} R_{bj} R_{ck} \chi_{ijk}(2\omega, \omega, \omega), \tag{S7}$$

$$\gamma_{abcd}(2\omega, \omega, \omega, 0) = \sum_{ijkl} R_{ai} R_{bj} R_{ck} R_{dl} \Gamma_{ijkl}(2\omega, \omega, \omega, 0). \tag{S8}$$

$$\tag{S9}$$

Finite Field Versus Response Theory:

Using DALTON, we can compute the second hyperpolarizability within a response scheme. We have compared the laboratory second hyperpolarizability obtained using the Finite Field method (using 19 QM calculations) to the one using the response theory in Table S1 for some components of a molecule in the vacuum. Very good agreement is found: an error about 20 a.u. can be expected

due the numerical calculation for the second hyperpolarizability. Same results have been found for second hyperpolarizability calculation within the PE environment – data not shown. Hence, throughout the article, the values are rounded to tens of a.u.

Table S1: Second hyperpolarizability components in the laboratory frame for a water molecule in vacuum, in atomic units. The results obtained by the Finite Field method presented in the main text and the one provided by `DALTON` using the response theory are compared. The calculations have been made at 2 fundamental wavelength: 800 nm and the infinity wave-length limit.

$\Gamma(2\omega,\omega,\omega,0)$	$\lambda = 800$ nm		$\lambda \rightarrow +\infty$ nm	
	Response	Finite Field	Response	Finite Field
Γ_{xxxx}	2604	2632	2094	2111
Γ_{xxyy}	744	745	583	584
Γ_{xyyx}	725	731	583	587
Γ_{xyxy}	744	745	583	584
Γ_{xxzz}	978	978	790	789
Γ_{xzzx}	965	969	790	784
Γ_{xzxz}	978	978	790	789
Γ_{yyxx}	693	698	583	587
Γ_{yxxy}	699	700	583	584
Γ_{yxyx}	693	698	583	587
Γ_{yyyy}	1234	1233	1054	1054
Γ_{yyzz}	818	816	680	678
Γ_{yzzy}	827	825	680	679
Γ_{yzyz}	818	816	680	678
Γ_{zzxx}	1025	1032	790	794
Γ_{zxxz}	988	987	790	789
Γ_{zxzx}	1025	1032	790	794
Γ_{zzyy}	916	916	680	679
Γ_{zyyz}	876	873	680	677
Γ_{zyzy}	916	916	680	679
Γ_{zzzz}	3491	3476	2719	2710

Comparison with Literature:

To conclude methodological checks, we have compared our results with the ones obtained in the literature. First, with the gold standard, Couple Cluster Single Double (CCSD), in the vacuum

phase. We compare our results with two recent works by Liang *et. al.*[1] and Beaujean *et. al.*[2] using CCSD with the d-aug-cc-pVTZ basis set at zero frequency. Table S2 compares components at zero frequency. Table S3 compares the experimentally relevant $\gamma_\parallel$, γ_{THS} or DR_{THS} that are defined as:

$$\gamma_\parallel = \frac{1}{15} \sum_{i,j} \gamma_{iijj} + \gamma_{ijij} + \gamma_{ijji}, \tag{S10}$$

$$\gamma_{THS} = \sqrt{\Gamma_{zzzz}^2 + \Gamma_{zxxx}^2}, \tag{S11}$$

$$DR_{THS} = \Gamma_{zzzz}^2 / \Gamma_{zxxx}^2. \tag{S12}$$

Indeed, these reduced values appear in scattering experiments since the experimental results cannot provide directly individual components. For complete γ_{THS} and DR_{THS} expressions, see Ref[3] for instance.

The difference observed characterize the error made due to DFT/CAM-B3LYP instead of CCSD and is comparable for the first and second hyperpolarizability: around 10%. An important point is the large frequency dependence of the second hyperpolarizability, see Table S3, which is quite well reproduced by DFT. We can also note the recent work of Besalú-Sala[4] which provides advice for tuning DFT functional to get γ closer to CCSD ones. They mention that DFT/CAMB3LYP is the best standard functional to use for water in vacuum, and that it overestimates the γ.

Regarding the liquid phase, the work by Osted *et.al.*[5] provides a prediction for the water second hyperpolarizability. We are using the same methodology but with more approximation: (1) they used CCSD with the same basis ; (2) Their MD simulation has been made using a polarizable force field ; (3) Their electrostatic embedding also include a polarizable part while we are not. They propose an pure electric $\gamma_\parallel(2\omega,\omega,\omega,0) = 2070$ a.u. at $\lambda \approx 1080$ nm. They compare this result by the one proposed by Levine and Bethea:[6] $\gamma_\parallel(2\omega,\omega,\omega,0) = 2134$ a.u. at the same frequency. We find, $\gamma_\parallel(2\omega,\omega,\omega,0)$ equal to 1730 a.u at 800nm and 1440 a.u at infinite wavelength. Our result is close to the experimental one, but is too small. However, in the liquid phase decreasing the wavelength seems to increase $\gamma_\parallel$. At 1080 nm we may hope our liquid $\gamma_\parallel$ to be closer than the

Table S2: **Water second hyperpolarizability in vacuum phase, in atomic unit, in the static limit. Our results (DFT/CAMB3LYP) are compared to the ones obtained by Liang _et. al._[1] (CCSD).**

γ	Zero frequency	
	CCSD[1]	DFT/CAMB3LYP
γ_{aaaa}	863	965
γ_{aabb}	654	763
γ_{bbbb}	2711	3156
γ_{caac}	450	507
γ_{cbbc}	724	828
γ_{cccc}	1506	1678
$\gamma_{\parallel}$	1747	1998
γ_{THS}	1794	2090
DR_{THS}	73	70

Table S3: **Water second hyperpolarizability in vacuum, in atomic unit. Our results (DFT/CAMB3LYP) are compared to the ones obtained by Beaujean _et. al._[2] (CCSD). Several wave-length of calculation are shown, in nanometer. We also observe that γ_{THS} increases with decreasing frequency while the depolarization ratio decreases.**

	CCSD[2]		DFT/CAMB3LYP	
Frequency [nm]	γ_{THS} [a.u.]	DR_{THS}	γ_{THS} [a.u.]	DR_{THS}
$+\inf$	1821	76	2090	70
1064	2288	49	NA	NA
800	NA	NA	2640	47
694.3	3401	24	NA	NA

experimental value.

S1.2 Convergence of β and γ relative to the configuration number

In Figure S2 and S3 the evolution of the mean values of the first and second hyperpolarizabilities at 800 nm are plotted as a function of the number of configurations used for the averaging. For every component, the evolution is compared to the last value (using 2400 configurations). Respectives errors of about 0.05 a.u. and 10 a.u. can be expected for the first and second hyperpolarizabilities due to the configuration averaging – which is far less than the error made using DFT. Finally, we
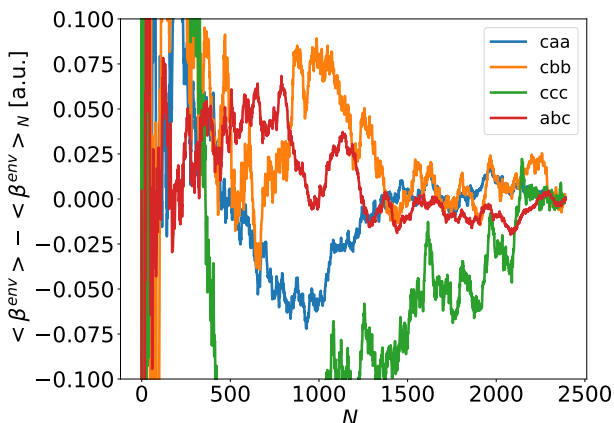

Figure S2: Convergence of $\langle \beta^{\mathrm{env}} \rangle$ relative to the number of configurations used. The reference value is given for N=2400 configurations.

have also checked that the sample obtained using these 2400 configurations is isotropic. Indeed, in top of the symmetry verification of the second hyperpolarizability, see the next section, the first hyperpolarizability in the laboratory frame has been computed. This tensor should be strictly null in average, because of the inversion symmetry inherent to the bulk phase. We obtained indeed a maximal average of 0.2 a.u. for all components.
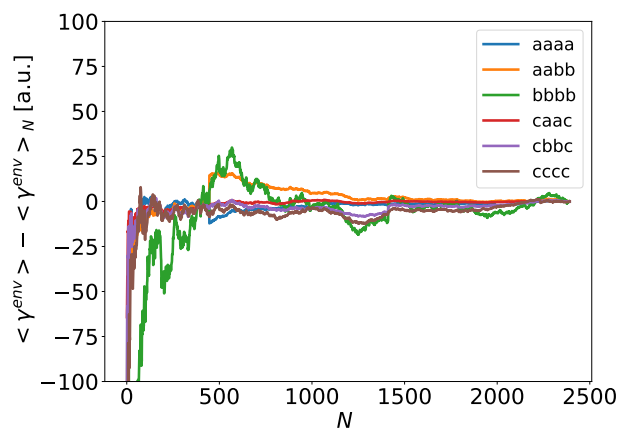
Figure S3: Convergence of $\langle \gamma^{\mathrm{env}} \rangle$ relative to the number of configurations used. The reference value is given for N=2400 configurations.

S2 Second hyperpolarizability γ in the bulk phase

S2.1 Symmetry, averages and standard deviations of γ

Table S4 and S5 report the second hyperpolarizability values in the molecular and laboratory frames, respectively. Only the components larger than 15 a.u. in average are shown.

Due to the C_{2v} molecular symmetry of water, only few γ components should be different of zero. The components γ_{iiii} and the γ_{iijj} with all permutations, where i and j can be a, b, or c. Regarding the second hyperpolarizability in the laboratory frame Γ, the averages should represent a centro-symmetric system. Hence, all Γ_{pppp} should be similar to 3 times Γ_{ppqq} (with all permutations), where p and q can be the laboratory axis x, y, or z.[7]

In the molecular frame, the C_{2v} molecular symmetry is respected by our results. The symmetry forbidden components have averages that are smaller than 15 a.u., our typical statistical error ; they are not strictly zero, due to statistical inaccuracies. In the laboratory frame, the centro-symmetry is also fulfilled regarding the Γ components. It confirms that our sample of 2400 molecules represents a centro-symmetric medium.

Table S4: $\gamma(2\omega, \omega, \omega, 0)$ **value in the vacuum and in bulk at 800 nm. For the bulk phase, the average,** $\langle \gamma^{\text{env}} \rangle$**, and standard deviation,** $\sigma[\gamma^{\text{env}}]$**, are presented in atomic unit. Absent components, which correspond to the** C_{2v} **symmetry forbidden ones, are below 15 a.u. in averaged for the bulk phase. The** $\gamma_\parallel$ **is defined in Equation S10.**

γ	γ^{vac}	$\langle \gamma^{\text{env}} \rangle$	$\sigma[\gamma^{\text{env}}]$
γ_{aaaa}	1110	740	140
γ_{aabb}	930	640	200
γ_{aacc}	590	370	60
γ_{abab}	930	640	200
γ_{abba}	940	660	140
γ_{acac}	590	370	60
γ_{acca}	590	370	80
γ_{baab}	1000	680	220
γ_{baba}	1070	710	150
γ_{bbaa}	1060	710	150
γ_{bbbb}	4090	2940	650
γ_{bbcc}	1120	770	170
γ_{bcbc}	1120	770	170
γ_{bccb}	1060	750	200
γ_{caac}	610	380	60
γ_{caca}	610	380	80
γ_{cbbc}	1010	730	150
γ_{cbcb}	1010	720	180
γ_{ccaa}	610	380	80
γ_{ccbb}	1000	720	180
γ_{cccc}	2000	1400	230
$\gamma_\parallel$	2500	1730	

12

Table S5: **Second hyperpolarizability in the laboratory frame** $\Gamma(2\omega, \omega, \omega, 0)$ **in the liquid phase at 800 nm. The average and standard deviation are presented in atomic unit,** $\langle \Gamma^{\text{env}} \rangle$ **and** $\sigma[\Gamma^{\text{env}}]$ **respectively. Absent components, which correspond to the inversion symmetry forbidden ones, are bellows 15 a.u.**

Γ	$\langle \Gamma^{\text{env}} \rangle$	$\sigma[\Gamma^{\text{env}}]$
Γ_{xxxx}	1740	830
Γ_{xxyy}	580	150
Γ_{xxzz}	580	160
Γ_{xyxy}	580	150
Γ_{xyyx}	580	170
Γ_{xzxz}	580	160
Γ_{xzzx}	570	150
Γ_{yxxy}	580	150
Γ_{yxyx}	580	170
Γ_{yyxx}	580	170
Γ_{yyyy}	1740	690
Γ_{yyzz}	580	170
Γ_{yzyz}	580	170
Γ_{yzzy}	570	150
Γ_{zxxz}	570	150
Γ_{zxzx}	580	150
Γ_{zyyz}	570	170
Γ_{zyzy}	580	150
Γ_{zzxx}	580	150
Γ_{zzyy}	580	150
Γ_{zzzz}	1710	660

S2.2 Relationship between bulk and vacuum values of water γ

Figure S4 displays the mean values of the γ components in the bulk, with respect to their values in the vacuum phase. For all components, a ratio of about 0.7 is found: the electrostatic embedding seems to reduce the second hyperpolarizability in the same way for all components.
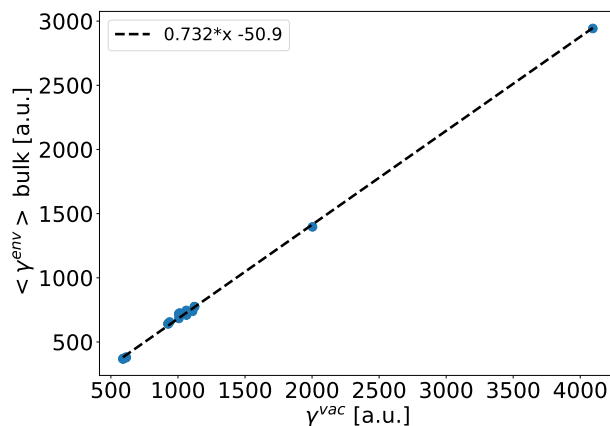

Figure S4: Mean value of the bulk non vanishing γ components as a function of their vacuum values. The dashed line represents a linear fit. The second hyperpolarizabilities are taken in the molecular frame.

S2.3 γ dispersity

Figure S5 presents the individual values of two β and γ components in the liquid phase: β_{yyy} in function of β_{zyy} and γ_{yyyz} in function of γ_{zzxx}. Due to the C_{2v} symmetry, β_{yyy} and γ_{yyyz} are null on average,while β_{zyy} and γ_{zzxx} have a non-zero average value. However, due to the wide dispersion of all these components, some molecules have larger β_{yyy} than β_{zyy}, or larger γ_{yyyz} than γ_{zzxx}.
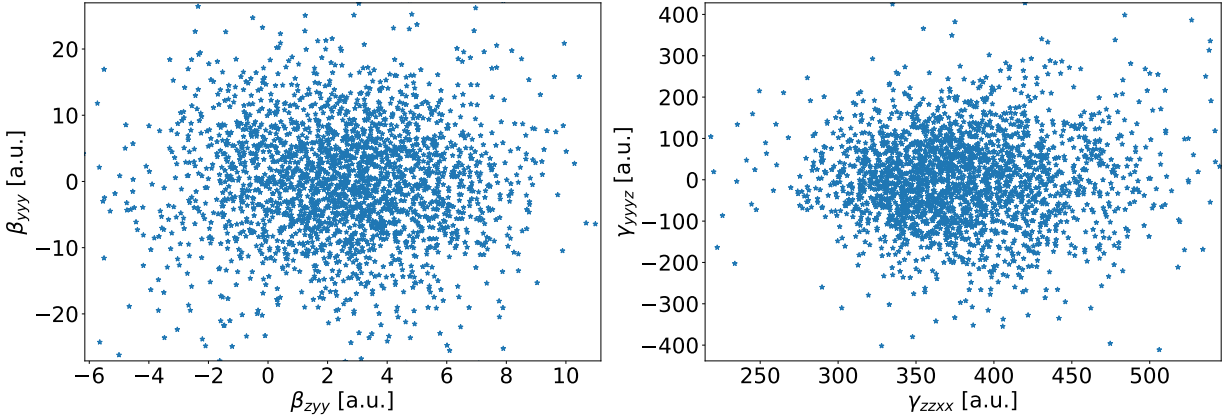
Figure S5: Distributions of some first and second hyperpolarizability components for liquid water. Each point represent one of the 2400 configurations of a water molecule in liquid water. Left : β_{yyy} in function of β_{zyy}. Right : γ_{yyyz} in function of γ_{zzxx}. Calculation for an excitation wavelength of 800 nm.

S3 Space heterogeneity of the Electrostatic field generated by the neighborhood

Here, we report the evolution of the spatial gradient of the electrostatic field generated by the PE embedding, depending on the environment size R_c. We have calculated

$$\langle |\Delta \delta e_i / \delta_j| \rangle (R_c) = \frac{1}{N} \sum_n \left| \left(\frac{\delta e_i}{\delta x_j} \right)^n [R_c] - \left(\frac{\delta e_i}{\delta x_j} \right)^n [R_f] \right|, \tag{S13}$$

where $\left(\frac{\delta e_i}{\delta x_j} \right)^n [R_c]$ is the spatial gradient along the molecular direction j of the electrostatic field along the direction i generated by an environment up to R_c around the molecule n. Figure S6 displays $\langle |\Delta \delta e_i / \delta_j| \rangle (R_c)$ with a logarithmic scale, and a reference gradient at $R_c = R_f = 40$ Å. According to the Figure S6, the total spatial gradient is quite large at small distance: about 10^{-2} a.u.. However, after few Angstroms, the neighborhood contribution to the spatial gradient drops.
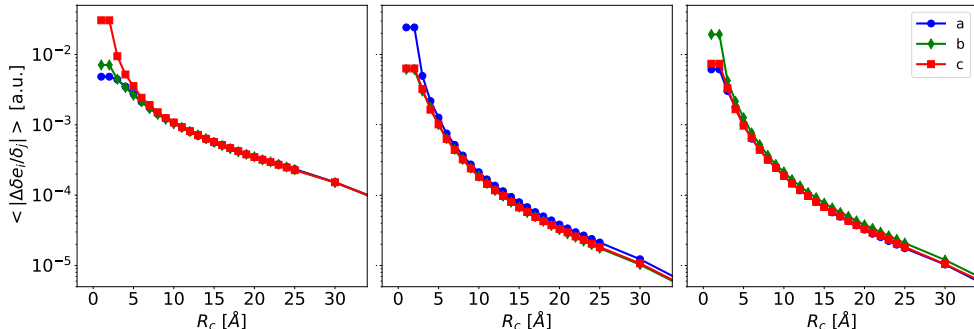

Figure S6: Evolution of the electrostatic gradient with respect to the environment size R_c. The averaged difference with respect to each molecule value at $R_c = R_f = 40$Åis plotted in logarithmic scale. The electrostatic field direction are represented by the 3 curves: along a (blue circle), b (green diamond) and c (orange square). The spatial direction of the derivative is presented from left to right: along the molecular axis a, b and c.

S4 γ-based correction: impact of γ fluctuations

In the main text, the same value of γ is attributed to all the water molecules to calculate our hyperpolarizability correction. To estimate the relevance of this approximation, 3 different ways of including the environment are compared here:

$$\beta^{PE}(R_c) = \beta^{PE}(R_c), \tag{S14}$$

$$\beta^{PE+L}(R_c) = \beta^{PE}(R_c) + \langle \gamma^{\mathrm{env}} \rangle \cdot \Delta \mathbf{e}(R_c), \tag{S15}$$

$$\beta^{PE+\gamma L}(R_c) = \beta^{PE}(R_c) + \gamma^{\mathrm{env}} \cdot \Delta \mathbf{e}(R_c). \tag{S16}$$

The QM/MM calculation up to a distance R_c, is noted $\beta^{PE}(R_c)$. The same $\beta^{PE}(R_c)$ but where the distant neighbors, between R_c and R_f are taken into account using the electric field they produced, $\Delta \mathbf{e}(R_c)$, using the averaged second hyperpolarizability $\langle \gamma^{\mathrm{env}} \rangle$ is noted $\beta^{PE+L}(R_c)$ and is presented in the main text. Finally, we also present here the results for $\beta^{PE+\gamma L}(R_c)$ that uses the individual values of the molecular second hyperpolarizability, instead of the averaged one.

Figure S7 presents the evolution of the average with respect to R_c and Figure S8 the $\Delta \beta_T$:

$$\Delta \beta_T^X = \frac{1}{27N} \sum_{ijk} \sum_{n=1}^{N} |\beta_{ijk}^{\mathrm{env}(n)} - \beta_{ijk}^{X(n)}|, \tag{S17}$$

also used in the main text. For the average, the result of β^{PE+L} and $\beta^{PE+\gamma L}$ are almost in top of each others. For R_c larger than about 5 Å, the results are converged. For the $\Delta \beta_T$, both corrections using $\Delta \mathbf{e}(R_c)$ are efficient. However, the $\beta^{PE+\gamma L}$ error decreases more rapidly: if the effect of the γ^{env} dispersion cannot be seen in the average predicted β, it is more important for individual value quantity such as $\Delta \beta_T$. However, increasing R_c using β^{PE+L} seems to achieve the same result as $\beta^{PE+\gamma L}$. Hence, using the averaged γ^{env} is justified for water in the liquid phase.
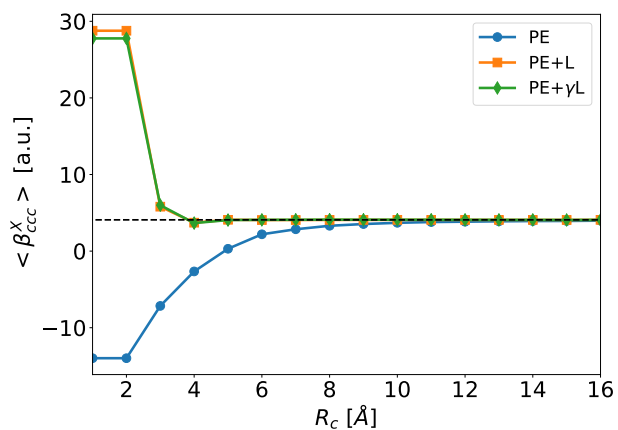
Figure S7: Evolution of the $\beta_{ccc}^X(R_c)$ averaged for the three corrections. The dashed line is the reference value obtained for $R_c = R_f = 4$ nm.
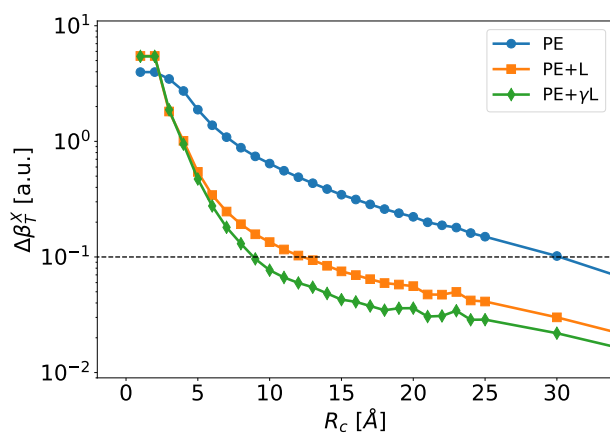

Figure S8: Evolution of the $\Delta\beta_T^X(R_c)$ for the three corrections. The dashed line represents the values at which convergence is considered to be obtained, and acts as a guide for the eyes.

References

(1) Liang, C.; Tocci, G.; Wilkins, D. M.; Grisafi, A.; Roke, S.; Ceriotti, M. Solvent fluctuations and nuclear quantum effects modulate the molecular hyperpolarizability of water. Phys. Rev. B **2017**, 96, 1–6.

(2) Beaujean, P.; Champagne, B. Coupled cluster investigation of the vibrational and electronic second and third harmonic scattering hyperpolarizabilities of the water molecule. J. Chem. Phys. **2019**, 151, 064303.

(3) Beaujean, P.; Champagne, B. Coupled cluster evaluation of the second and third harmonic scattering responses of small molecules. Theor. Chem. Acc. **2018**, 137, 50.

(4) Besalú-Sala, P.; Sitkiewicz, S. P.; Salvador, P.; Matito, E.; Luis, J. M. A new tuned range-separated density functional for the accurate calculation of second hyperpolarizabilities. Phys. Chem. Chem. Phys. **2020**, 22, 11871–11880.

(5) Osted, A.; Kongsted, J.; Mikkelsen, K. V.; Åstrand, P. O.; Christiansen, O. Statistical mechanically averaged molecular properties of liquid water calculated using the combined coupled cluster/molecular dynamics method. J. Chem. Phys. **2006**, 124, 124503.

(6) Levine, B.; Bethea, C. Effects on hyperpolarizabilities of molecular interactions in associating liquid mixtures. J. Chem. Phys. **1976**, 65, 2429–2438.

(7) Brevet, P.-F. In Surface Second Harmonic Generation; Romandes, P. P., Ed.; 1997.

List of Footnotes